Sparse Tensor Discriminant Color Space for Face Verification

Su-Jing Wang, Jian Yang, *Member, IEEE*, Ming-Fang Sun, Xu-Jun Peng, Ming-Ming Sun, and Chun-Guang Zhou

***Abstract*— As one of the fundamental features, color provides useful information and plays an important role for face recognition. Generally, the choice of a color space is different for different visual tasks. How can a color space be sought for the specific face recognition problem? To address this problem, we propose a sparse tensor discriminant color space (STDCS) model that represents a color image as a third-order tensor in this paper. The model cannot only keep the underlying spatial structure of color images but also enhance robustness and give intuitionistic or semantic interpretation. STDCS transforms the eigenvalue problem to a series of regression problems. Then one spare color space transformation matrix and two sparse discriminant projection matrices are obtained by applying lasso or elastic net on the regression problems. The experiments on three color face databases, AR, Georgia Tech, and Labeled Faces in the Wild face databases, show that both the performance and the robustness of the proposed method outperform those of the state-of-the-art TDCS model.**

***Index Terms*— Color images, discriminant information, face recognition, sparse representation, tensor subspace.**

I. Introduction

AFTER decades of research and development, face recognition has attained considerable success in the field of personal identification and public security, such as crime and terrorist recognition. The various face recognition methods attract great interests from researchers. Some of them focus on how to extract the effective features from facial images. Principal component analysis (PCA) [1] and linear discriminant analysis (LDA) [2] are two popular methods for feature extraction. To keep the spatial structure information of facial images, 2-D PCA (2-D-PCA) [3] and 2-D LDA (2-D-LDA) [4] directly computed covariance (scatter) matrices from the image matrix. Recently, the feature extraction methods based on tensor is a hot topic. The methods can be divided into two categories. In one category [5]–[7], a high order tensor constructs a multilinear structure, and models the multiple factors of facial variation (e.g., different user identities, various user postures and facial expressions, varying lights, etc.) using high-order singular value decomposition (HOSVD) [8]–[10]. In the other category [11]–[14], the conventional transformation methods (such as PCA, SVD) and locality preserving projections [15] are generalized to tensors. They treat a gray image as a second-order tensor, a color image as a third-order tensor.

Some of researchers focus on how to design novel classifiers for face recognition. Kumar *et al.* [16] created the first image search engine based entirely on faces. They divided the face into various regions and extracted the features from these regions. Then, support vector machine and Adaboost were used to classify attributes by various combinations of these regions. Wright *et al.* [17] developed a classifier based on sparse solution to enhance the performance of occluded face recognition. Schwartz *et al.* [18] developed a classifier based on partial least squares and discriminative tree to accelerate face identification for large data sets. To deal well with the large-scale and high-dimensional data sets, Fan *et al.* [19] used the sample neighbors to effectively captures the structures of the data and may enhance the face recognition result. Zafeiriou *et al.* [20] used regularized kernel discriminant analysis to enhance face recognition and verification.

However, many methods only use gray-scale information of face images. Thus plenty of color information, which is useful for face recognition according to recent researches [21]–[24], is lost. In [21], the experimental results showed that the recognition accuracy was improved if color information was available for PCA-based methods. In [22], a RGB image whose size was $I_1 \times I_2$ transformed into a $I \times 3$ matrix ($I = I_1 \times I_2$), and the 2-D-PCA was applied on all transformed matrices to recognize the color face images. The experimental results showed that the accuracy can be improved by about 3% compared to the same method, which was applied on the corresponding gray-scale images. It was demonstrated by Choi *et al*. [23] that the recognition performance can be significantly improved for low resolution face images (20×20 pixels or

Manuscript received May 21, 2011; revised March 15, 2012; accepted March 17, 2012. Date of publication April 10, 2012; date of current version May 10, 2012. This work was supported in part by the National Natural Science Foundation of China, under Grant 60973092, Grant 60903097, and Grant 61175023, the Key Laboratory for Symbol Computation and Knowledge Engineering of the National Education Ministry of China, the National Science Foundation of China, under Grant 60973098 and Grant 61005005, and the National Science Fund for Distinguished Young Scholars under Grant 61125305.

S.-J. Wang, M.-F. Sun, and C.-G. Zhou are with the College of Computer Science and Technology, Jilin University, Changchun 130012, China (e-mail: wangsj08@mails.jlu.edu.cn; sunmf09@mails.jlu.edu.cn; Corresponding author: cgzhou@jlu.edu.cn).

J. Yang is with the School of Computer Science and Technology, Nanjing University of Science and Technology, Nanjing 210094, China, and also with the Computation and Neural Systems, California Institute of Technology, Pasadena, CA 91125 USA (e-mail: csjyang@njit.edu).

X.-J. Peng is with Raytheon BBN Technologies, Cambridge, MA 02138 USA (e-mail:xpeng@bbn.com).

M.-M. Sun is with the School of Computer Science and Technology, Nanjing University of Science and Technology, Nanjing 210094, China (e-mail: sunmingming@gmail.com).

Color versions of one or more of the figures in this paper are available online at http://ieeexplore.ieee.org.

Digital Object Identifier 10.1109/TNNLS.2012.2191620

less) using facial color cue. Other researches [24] also reveal that different color spaces (such as RGB, PCA color space, and YIQ color space) provide better face recognition performance than gray scale only.

In computer vision field, most color spaces can be defined by a transformation of the RGB color space, which is the most widely used color space. The linear transformation color spaces, such as the YUV and YIQ color space [25], are usually associated with the properties of some hardwares. While the nonlinear transformation color spaces, such as the HSV and L*a*b* color space, are generally related to the human vision system.

Usually, the R, G, and B component images in the RGB color space are correlated. Decorrelation among the components of component images helps to reduce redundancy, and is an important strategy to improve the accuracy of the subsequent recognition method [26]. Liu [27] proposed the uncorrelated color space (UCS), the independent color space (ICS), and the discriminating color space (DCS). Specifically, the UCS applies PCA to decorrelate the R, G, and B component images. The ICS and DCS further enhance the discriminating power for the subsequent recognition method by means of independent component analysis (ICA) and LDA, respectively.

When an optimal color space is obtained, its effectiveness is evaluated by using a recognition method. This separate strategy cannot theoretically guarantee that the optimal color space is best for the subsequent recognition method, and therefore, cannot guarantee that the resulting face recognition system is optimal in performance. Color image discriminant (CID) model [28] is to seek a m optimal color space and an effective recognition method of color images in a unified framework. However, CID vectorizes each component image into a high-dimensional vector. This results in the loss of spatial structure information of the component images. Moreover, CID also suffers from the small sample size problem. To overcome these drawbacks, Wang *et al.* [29] presented a tensor DCS (TDCS) model, which used a third-order tensor to represent a color facial image.

Now, we review the above algorithms from the feature selection (or rather, the feature transformation) view. UCS, ICS, and DCS are the results of feature transformations by using PCA, ICA, and LDA on the RGB color components. CID used LDA not only on the RGB color components but also on image information. To keep more spatial structure information of the component images, TDCS use discriminant analysis with tensor representation to transform the RGB color components and the image information.

Unfortunately, there is a lot of noise on real data. So, the above feature transformations cannot obtain the best performance on real data. We can impose a sparse constraint on their object functions. The sparseness is a trade-off between the optimal solution of their object functions and the noises.

Recently, the sparse feature transformation is one of the hottest topics. Many papers show that the sparse feature transformation methods can obtain better performance than their corresponding non-sparse methods in the real data. And these sparse methods can give an intuitionistic or semantic interpretation for the transformed subspace. Sparse PCA (SPCA) was first proposed in [30] by applying the least angle regression [31] and elastic net of ℓ_1-penalized regression [32] on regular principal components. In [33], Moghaddam *et al*. suggested a spectral bounds framework for sparse subspace learning, and presented both exact and greedy algorithms for sparse LDA (SLDA). They also described the same framework for SPCA but they can only be applied to two-class problem [34]. In order to address this problem, Qiao *et al*. [35] extended the SPCA to obtain sparse discriminant vectors.

In this paper, we draw upon the insight from these approaches and explore a STDCS model which is an extension of TDCS [29]. The aim of sparse TDCS (STDCS) is to make two discriminant projection matrices U_1, U_2 and one color space transformation matrix U_3 sparse. Compared to the TDCS model, STDCS has two main advantages: 1) the intuitionistic or semantic interpretation and 2) the robustness not only for similarity measurement of images but also for noised images.

The rest of this paper is organized as follows. In Section II, we give the related definitions to tensor. In Section III, we will briefly review the TDCS model, which is followed by an introduction of the STDCS model in Section IV. In Section V, the experiments are conducted on three color face databases: AR, Georgia Tech, and labeled faces in the wild (LFW) face databases, and the results are covered in the same section, which show that the efficiency and performance of STDCS are better than those of TDCS and CID. Finally in Section VI, conclusions are drawn and several issues for the future works are described.

II. Tensor Fundamentals

A tensor is a multidimensional array. It is the higher order generalization of scalar (zero-order tensor), vector (first-order tensor), and matrix (second-order tensor). In this paper, lowercase italic letters (*a, b,…*) denote scalars, bold lowercase letters (**a, b,…**) denote vectors, bold uppercase letters (**A, B,…**) denote matrices, and calligraphic uppercase letters ($\mathcal{A}$, $\mathcal{B}$, …) denote tensors. The formal definition is given below [10].

Definition 1: The *order* of a tensor $\mathcal{A} \in \mathbb{R}^{I_1 \times I_2 \times \cdots \times I_N}$ is N. An element of $\mathcal{A}$ is denoted by $\mathcal{A}_{i_1 i_2 \ldots i_N}$ or $a_{i_1 i_2 \ldots i_N}$, where $1 \leq i_n \leq I_n$, $n = 1, 2, \ldots, N$.

Definition 2: The *n-mode vectors* of $\mathcal{A}$ are the I_n-dimensional vectors obtained from $\mathcal{A}$ by fixing every index but index i_n.

Definition 3: The *n-mode unfolding matrix* of $\mathcal{A}$, denoted by $(\mathcal{A})_{(n)} \in \mathbb{R}^{I_n \times (I_1 \ldots I_{n-1} I_{n+1} \ldots \times I_N)}$, contains the element $a_{i_1 \ldots i_N}$ at i_nth row and at jth column, where

$$j = 1 + \sum_{k=1, k \neq n}^{N} (i_k - 1) J_k, \quad \text{with} \quad J_k = \prod_{m=1, m \neq n}^{k-1} I_m. \quad (1)$$

We can generalize the product of two matrices to the product of a tensor and a matrix.

Definition 4: The *n-mode product* of a tensor $\mathcal{A} \in \mathbb{R}^{I_1 \times I_2 \times \cdots \times I_N}$ by a matrix $\mathbf{U} \in \mathbb{R}^{J_n \times I_n}$, denoted by $\mathcal{A} \times_n \mathbf{U}$, is an $(I_1 \times I_2 \times \cdots \times I_{n-1} \times J_n \times I_{n+1} \times \cdots \times I_N)$-tensor of

which the entries are given by:

$$(\mathcal{A} \times_n \mathbf{U})_{i_1 i_2 \ldots i_{n-1} j_n i_{n+1} \ldots i_N} \stackrel{\text{def}}{=} \sum_{i_n} a_{i_1 i_2 \ldots i_{n-1} i_n i_{n+1} \ldots i_N} u_{j_n i_n}. \quad (2)$$

Definition 5: The *scalar product* of two tensors $\mathcal{A}, \mathcal{B} \in \mathbb{R}^{I_1 \times I_2 \times \cdots \times I_N}$, denoted by $\langle \mathcal{A}, \mathcal{B} \rangle$, is defined in a straightforward way as $\langle \mathcal{A}, \mathcal{B} \rangle \stackrel{\text{def}}{=} \sum_{i_1} \sum_{i_2} \cdots \sum_{i_N} a_{i_1 i_2 \ldots i_N} b_{i_1 i_2 \ldots i_N}$. The *Frobenius norm* of a tensor $\mathcal{A} \in \mathbb{R}^{I_1 \times I_2 \times \cdots \times I_N}$ is then defined as $\|\mathcal{A}\|_F \stackrel{\text{def}}{=} \sqrt{\langle \mathcal{A}, \mathcal{A} \rangle}$.

Form the definition of the n-mode unfolding matrix, we have

$$\|\mathcal{A}\|_F = \|(\mathbf{A})_{(n)}\|_F. \quad (3)$$

By using tensor decomposition, any tensor $\mathcal{A}$ can be expressed as the product

$$\mathcal{A} = \mathcal{C} \times_1 \mathbf{U}_1 \times_2 \mathbf{U}_2 \cdots \times_N \mathbf{U}_N \quad (4)$$

where $\mathbf{U}_n$, $n = 1, 2, \ldots, N$, is an orthonormal matrix and contains the ordered principal components for the nth mode. $\mathcal{C}$ is called the *core tensor*. Unfolding the above equation, we have

$$\mathbf{A}_{(n)} = \mathbf{U}_n \mathbf{C}_{(n)} (\mathbf{U}_N \otimes \cdots \otimes \mathbf{U}_{n+1} \otimes \mathbf{U}_{n-1} \otimes \cdots \otimes \mathbf{U}_1)^T \quad (5)$$

where operator $\otimes$ is the Kronecker product of the matrices.

III. Overview of Tensor Discriminant Color Space Model

In this section, we overview the TDCS model. In TDCS, a color image is naturally represented by a third-order tensor. The 1-mode of a tensor is the height of an image, the 2-mode of a tensor is the width of an image, and the 3-mode of tensor is the color space of an image. For instance, a RGB image with size $I_1 \times I_2$ is represented as a tensor $\mathcal{A} \in \mathbb{R}^{I_1 \times I_2 \times I_3}$, where $I_3 = 3$. The 3-mode of $\mathcal{A}$ is the color variable in the RGB color space, which has three components corresponding to **R**, **G**, and **B** in RGB space.

Assuming C is the number of individuals, $\mathcal{A}_i^c$ is the ith color face image of cth individual, and M_c is the number of color face images of cth individual, where $M = M_1 + M_2 + \cdots + M_C$. The TDCS algorithm seeks two discriminant projection matrices $\mathbf{U}_1 \in \mathbb{R}^{I_1 \times L_1}$, $\mathbf{U}_2 \in \mathbb{R}^{I_2 \times L_2}$ and a color space transformation matrix $\mathbf{U}_3 \in \mathbb{R}^{I_3 \times L_3}$ (usually $L_1 < I_1$, $L_2 < I_2$, and $L_3 \leq I_3$) for transformation

$$\mathcal{D}_i^c = \mathcal{A}_i^c \times_1 \mathbf{U}_1^T \times_2 \mathbf{U}_2^T \times_3 \mathbf{U}_3^T, \quad i = 1, 2, \ldots, M_c, \quad c = 1, 2, \ldots, C \quad (6)$$

which ensures that the projected tensors from the same individual are distributed as close as possible, while the projected tensors from different individuals are distributed as far as possible.

The mean image of the cth individual is defined by

$$\overline{\mathcal{A}}^c = \frac{1}{M_c} \sum_{i=1}^{M_c} \mathcal{A}_i^c \quad (7)$$

and the mean image of all individuals is defined by

$$\overline{\mathcal{A}} = \frac{1}{C} \sum_{c=1}^{C} \overline{\mathcal{A}}^c. \quad (8)$$

The between-class scatter of color images is defined as

$$\Psi_b(\mathcal{A}) = \sum_{c=1}^{C} \|\overline{\mathcal{A}}^c - \overline{\mathcal{A}}\|_F^2 \quad (9)$$

and within-class scatter of color images is defined as

$$\Psi_w(\mathcal{A}) = \sum_{c=1}^{C} \sum_{i=1}^{M_c} \|\mathcal{A}_i^c - \overline{\mathcal{A}}^c\|_F^2. \quad (10)$$

A reasonable idea is to maximize the between-class scatter of projected tensors $\Psi_b(\mathcal{D})$ and to minimize the within-class scatter of projected tensors $\Psi_w(\mathcal{D})$. Then TDCS criterion can be defined as follows:

$$\max J(\mathbf{U}_1, \mathbf{U}_2, \mathbf{U}_3) = \frac{\Psi_b(\mathcal{D})}{\Psi_w(\mathcal{D})}. \quad (11)$$

Here, three matrices $\mathbf{U}_n$ need to be simultaneously updated for achieving the optimal solution of the criterion function J. We can define n-mode between-class scatter matrix $\mathbf{S}_b^{(n)}$ and n-mode within-class scatter matrix $\mathbf{S}_w^{(n)}$ as

$$\mathbf{S}_b^{(n)} = \sum_{c=1}^{C} \left(\overline{\mathbf{A}}_{(n)}^c - \overline{\mathbf{A}}_{(n)}\right) \tilde{\mathbf{U}}_n \tilde{\mathbf{U}}_n^T \left(\overline{\mathbf{A}}_{(n)}^c - \overline{\mathbf{A}}_{(n)}\right)^T \quad (12)$$

and

$$\mathbf{S}_w^{(n)} = \sum_{c=1}^{C} \sum_{i=1}^{M_c} \left(\mathbf{A}_{i(n)}^c - \overline{\mathbf{A}}_{(n)}^c\right) \tilde{\mathbf{U}}_n \tilde{\mathbf{U}}_n^T \left(\mathbf{A}_{i(n)}^c - \overline{\mathbf{A}}_{(n)}^c\right)^T \quad (13)$$

where $\tilde{\mathbf{U}}_n = \mathbf{U}_N \otimes \cdots \otimes \mathbf{U}_{n+1} \otimes \mathbf{U}_{n-1} \otimes \cdots \otimes \mathbf{U}_1$, $n = 1, 2, \ldots, N$ and $N = 3$.

Then, the between-class scatter of the projected tensors $\Psi_b(\mathcal{D})$ and the within-class scatter of the projected tensors $\Psi_w(\mathcal{D})$ can be rewritten as follows:

$$\Psi_b(\mathcal{D}) = tr\left(\mathbf{U}_n^T \mathbf{S}_b^{(n)} \mathbf{U}_n\right) \quad (14)$$

and

$$\Psi_w(\mathcal{D}) = tr\left(\mathbf{U}_n^T \mathbf{S}_w^{(n)} \mathbf{U}_n\right). \quad (15)$$

So, given all other projection matrices $\mathbf{U}_1, \ldots, \mathbf{U}_{n-1}, \mathbf{U}_{n+1}, \ldots, \mathbf{U}_N$, the TDCS criterion can be written as follows:

$$\max \frac{tr\left(\mathbf{U}_n^T \mathbf{S}_b^{(n)} \mathbf{U}_n\right)}{tr\left(\mathbf{U}_n^T \mathbf{S}_w^{(n)} \mathbf{U}_n\right)}. \quad (16)$$

According to Rayleigh quotient, (16) is maximized if and only if the matrix $\mathbf{U}_n$ consists of L_n generalized eigenvectors, which are corresponding to the largest L_n generalized eigenvalues of the matrix pencil $(\mathbf{S}_b^{(n)}, \mathbf{S}_w^{(n)})$, which satisfies

$$\mathbf{S}_b^{(n)} \mathbf{v} = \lambda \mathbf{S}_w^{(n)} \mathbf{v}. \quad (17)$$

Since $\mathbf{S}_b^{(n)}$ and $\mathbf{S}_w^{(n)}$ are dependent on $\mathbf{U}_1, \ldots, \mathbf{U}_{n-1}, \mathbf{U}_{n+1}, \ldots, \mathbf{U}_N$, we can see that the optimization of $\mathbf{U}_n$ depends on the projections of other modes. An iterative procedure can be constructed to maximize (11). For details, please refer to our previous work [29].

IV. STDCS Model

In this section, we discuss how to model the STDCS. The same symbols described and defined in Section III are re-used. The aim of STDCS is not only to maximize (11) but also to make three matrices $\mathbf{U}_n$ sparse. Here, sparsity means that $\mathbf{U}_n$ has only a small number of nonzero elements or it has lots of zero elements. Therefore, the criterion function of STDCS is defined as

$$\begin{aligned} &\max J(\mathbf{U}_1, \mathbf{U}_2, \mathbf{U}_3) = \frac{\Psi_b(\mathcal{D})}{\Psi_w(\mathcal{D})} \\ &\text{s.t.} \quad Card(\mathbf{U}_n) < K_n, \quad n = 1, 2, 3 \end{aligned} \tag{18}$$

where $Card(\cdot)$ denotes the number of nonzero elements of $\mathbf{U}_n$. The only difference between (11) and (18) is a sparseness constraint imposed in (18). We convert the generalized eigenvalue problem (16) to a regression problem and then apply penalized least squares with an ℓ_1 penalty. We combine all color face images $\mathcal{A}_i^c \in \mathbb{R}^{I_1 \times I_2 \times 3}$ into a fourth-order tensor $\mathcal{A} \in \mathbb{R}^{I_1 \times I_2 \times 3 \times M}$. To facilitate the subsequent discussion, two tensors $\mathcal{H}_w \in \mathbb{R}^{I_1 \times I_2 \times 3 \times M}$ and $\mathcal{H}_b \in \mathbb{R}^{I_1 \times I_2 \times 3 \times M}$ are introduced as follows:

$$\mathcal{H}_w = \left\{ \begin{array}{c} (\mathcal{A}_1^1 - \overline{\mathcal{A}}^1) \\ \vdots \\ (\mathcal{A}_{M_1}^1 - \overline{\mathcal{A}}^1) \\ (\mathcal{A}_1^2 - \overline{\mathcal{A}}^2) \\ \vdots \\ (\mathcal{A}_{M_2}^2 - \overline{\mathcal{A}}^2) \\ \vdots \\ (\mathcal{A}_1^C - \overline{\mathcal{A}}^C) \\ \vdots \\ (\mathcal{A}_{M_C}^C - \overline{\mathcal{A}}^C) \end{array} \right\} \quad \text{and} \quad \mathcal{H}_b = \left\{ \begin{array}{c} (\overline{\mathcal{A}}^1 - \overline{\mathcal{A}}) \\ \vdots \\ (\overline{\mathcal{A}}^1 - \overline{\mathcal{A}}) \\ (\overline{\mathcal{A}}^2 - \overline{\mathcal{A}}) \\ \vdots \\ (\overline{\mathcal{A}}^2 - \overline{\mathcal{A}}) \\ \vdots \\ (\overline{\mathcal{A}}^C - \overline{\mathcal{A}}) \\ \vdots \\ (\overline{\mathcal{A}}^C - \overline{\mathcal{A}}) \end{array} \right\} \tag{19}$$

where $\{\cdot\}$ denotes the combination of M Nth order tensors into a $(N+1)$th order tensor. Further, $\mathcal{H}_b$ can be reduced to a lower dimension tensor $\mathcal{H}_b' \in \mathbb{R}^{I_1 \times I_2 \times 3 \times C}$ according to

$$\mathcal{H}_b' = \left\{ \begin{array}{c} (\overline{\mathcal{A}}^1 - \overline{\mathcal{A}}) \\ (\overline{\mathcal{A}}^2 - \overline{\mathcal{A}}) \\ \vdots \\ (\overline{\mathcal{A}}^C - \overline{\mathcal{A}}) \end{array} \right\}. \tag{20}$$

Theorem 1: Given $N-1$ projection matrices $\mathbf{U}_1, \ldots, \mathbf{U}_{n-1}$, $\mathbf{U}_{n+1}, \ldots, \mathbf{U}_N$, let

$$\mathcal{G}_w = \mathcal{H}_w \times_1 \mathbf{U}_1 \ldots \times_{n-1} \mathbf{U}_{n-1} \times_{n+1} \mathbf{U}_{n+1} \ldots \times_N \mathbf{U}_N \tag{21}$$

$$\mathcal{G}_b = \mathcal{H}_b \times_1 \mathbf{U}_1 \ldots \times_{n-1} \mathbf{U}_{n-1} \times_{n+1} \mathbf{U}_{n+1} \ldots \times_N \mathbf{U}_N \tag{22}$$

and

$$\mathcal{G}_b' = \mathcal{H}_b' \times_1 \mathbf{U}_1 \ldots \times_{n-1} \mathbf{U}_{n-1} \times_{n+1} \mathbf{U}_{n+1} \ldots \times_N \mathbf{U}_N. \tag{23}$$

Then, $\mathbf{S}_w^{(n)} = \mathbf{G}_{w(n)} \mathbf{G}_{w(n)}^T$, $\mathbf{S}_b^{(n)} = \mathbf{G}_{b(n)} \mathbf{G}_{b(n)}^T$, and $\mathbf{S}_b^{(n)} = \mathbf{G}_{b(n)}' \mathbf{G}_{b(n)}'^T$.

Proof: Apply n-mode unfolding on (22)

$$\mathbf{G}_{b(n)}' = (\mathcal{H}_b \times_1 \mathbf{U}_1 \ldots \times_{n-1} \mathbf{U}_{n-1} \times_{n+1} \mathbf{U}_{n+1} \ldots {}_N\mathbf{U}_N)_{(n)}. \tag{24}$$

For c-th class

$$\left((\overline{\mathcal{A}}^c - \overline{\mathcal{A}}) \times_1 \mathbf{U}_1 \ldots \times_{n-1} \mathbf{U}_{n-1} \times_{n+1} \mathbf{U}_{n+1} \ldots {}_N\mathbf{U}_N\right)_{(n)} = (\overline{\mathcal{A}^c} - \overline{\mathcal{A}})_{(n)} \cdot \widetilde{\mathbf{U}}_n. \tag{25}$$

Obviously, $\mathbf{G}_{b(n)}'$ can be rewritten as

$$\mathbf{G}_{b(n)}' = \left[(\overline{\mathcal{A}}^1 - \overline{\mathcal{A}})_{(n)} \cdot \widetilde{\mathbf{U}}_n, (\overline{\mathcal{A}}^2 - \overline{\mathcal{A}})_{(n)} \cdot \widetilde{\mathbf{U}}_n, \ldots, (\overline{\mathcal{A}}^C - \overline{\mathcal{A}})_{(n)} \cdot \widetilde{\mathbf{U}}_n \right]. \tag{26}$$

So

$$\begin{aligned} \mathbf{G}_{b(n)}' \mathbf{G}_{b(n)}'^T &= \left[(\overline{\mathcal{A}}^1 - \overline{\mathcal{A}})_{(n)} \cdot \widetilde{\mathbf{U}}_n, \right. \\ &\quad \left. \times (\overline{\mathcal{A}}^2 - \overline{\mathcal{A}})_{(n)} \cdot \widetilde{\mathbf{U}}_n, \ldots, (\overline{\mathcal{A}}^C - \overline{\mathcal{A}})_{(n)} \cdot \widetilde{\mathbf{U}}_n \right] \\ &\quad \cdot \begin{bmatrix} \widetilde{\mathbf{U}}_n^T \cdot (\overline{\mathcal{A}}^1 - \overline{\mathcal{A}})_{(n)}^T \\ \widetilde{\mathbf{U}}_n^T \cdot (\overline{\mathcal{A}}^2 - \overline{\mathcal{A}})_{(n)}^T \\ \vdots \\ \widetilde{\mathbf{U}}_n^T \cdot (\overline{\mathcal{A}}^C - \overline{\mathcal{A}})_{(n)}^T \end{bmatrix} \\ &= \sum_{c=1}^{C} (\overline{\mathcal{A}}^c - \overline{\mathcal{A}})_{(n)} \cdot \widetilde{\mathbf{U}}_n \cdot \widetilde{\mathbf{U}}_n^T \cdot (\overline{\mathcal{A}}^c - \overline{\mathcal{A}})_{(n)}^T \\ &= \sum_{c=1}^{C} (\overline{\mathcal{A}}_{(n)}^c - \overline{\mathcal{A}}_{(n)}) \cdot \widetilde{\mathbf{U}}_n \cdot \widetilde{\mathbf{U}}_n^T \cdot (\overline{\mathcal{A}}_{(n)}^c - \overline{\mathcal{A}}_{(n)})^T \\ &= \mathbf{S}_b^{(n)}. \end{aligned} \tag{27}$$

Similarly, we can prove $\mathbf{S}_w^{(n)} = \mathbf{G}_{w(n)} \mathbf{G}_{w(n)}^T$ and $\mathbf{S}_b^{(n)} = \mathbf{G}_{b(n)} \mathbf{G}_{b(n)}^T$. ■

Theorem 2: $\mathbf{S}_w^{(n)}$ is positive definite and its Cholesky decomposition is denoted as $\mathbf{S}_w^{(n)} = \mathbf{R}_{w(n)}^T \mathbf{R}_{w(n)}$, where $\mathbf{R}_{w(n)} \in \mathbb{R}^{I_n \times I_n}$ is an upper triangular matrix. $\mathbf{v}_1, \ldots, \mathbf{v}_{L_n}$ are eigenvectors of (17), which correspond to the L_n largest eigenvalues. $\mathbf{A} = [\alpha_1, \ldots, \alpha_{L_n}]$ and $\mathbf{B} = [\beta_1, \ldots, \beta_{L_n}]$ ($\mathbf{A} \in \mathbb{R}^{I_n \times L_n}$). For $\lambda > 0$, then $\hat{\mathbf{A}}$ and $\hat{\mathbf{B}}$ are the solutions of the following problems:

$$\begin{aligned} &\min_{\mathbf{A},\mathbf{B}} \sum_{i=1}^{\widetilde{I}_n} \|\mathbf{R}_{w(n)}^{-T} \mathbf{g}_i - \mathbf{A}\mathbf{B}^T \mathbf{g}_i\|^2 - \lambda \sum_{j=1}^{L_n} \beta_j^T \mathbf{S}_w^{(n)} \beta_j \\ &\text{s.t.} \quad \mathbf{A}^T \mathbf{A} = \mathbf{I} \end{aligned} \tag{28}$$

where $\widetilde{I}_n = I_1 \times \cdots \times I_{n-1} \times I(n+1) \times \cdots \times I_N \times M$ and $\mathbf{g}_i$ is the ith row of $\mathbf{G}_{b(n)}$. Then $\hat{\beta}_j$ spans the same linear space as $\mathbf{v}_j$, where $j = 1, \ldots, \text{Ł}_n$

Proof: The proof is similar to [35, Th. 1]. ■

According to Theorem 2, the generalized eigenvalue of (17) is transformed to the regression problem of (28). The regression problem (28) has two variables $\mathbf{A}, \mathbf{B}$ that need to be optimized simultaneously. It can be solved by iteratively minimizing over $\mathbf{A}$ and $\mathbf{B}$.

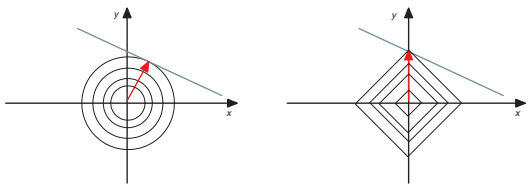

Fig. 1. Sparse solution can be found by solving a ℓ_1 norm problem but not by solving a traditional ℓ_2 norm problem. The x component of the solution of ℓ_1 norm is zero.

Given a fixed $\mathbf{B}$, the second term in (28) is constant. Its first term can be rewritten as

$$\begin{aligned}
&\sum_{i=1}^{\widetilde{I}_n} \|\mathbf{R}_{w(n)}^{-T}\mathbf{g}_i - \mathbf{A}\mathbf{B}^T\mathbf{g}_i\|^2 \\
&= \|\mathbf{G}_{b(n)}\mathbf{R}_{w(n)}^{-1} - \mathbf{G}_{b(n)}\mathbf{B}\mathbf{A}^T\|^2 \\
&= \mathrm{tr}[(\mathbf{G}_{b(n)}\mathbf{R}_{w(n)}^{-1} - \mathbf{G}_{b(n)}\mathbf{B}\mathbf{A}^T)(\mathbf{G}_{b(n)}\mathbf{R}_{w(n)}^{-1} - \mathbf{G}_{b(n)}\mathbf{B}\mathbf{A}^T)^T] \\
&= \mathrm{tr}(\mathbf{G}_{b(n)}\mathbf{R}_{w(n)}^{-1}\mathbf{R}_{w(n)}^{-T}\mathbf{G}_{b(n)}^T + \mathbf{G}_{b(n)}\mathbf{B}\mathbf{B}^T\mathbf{G}_{b(n)}^T) \\
&\quad -2tr(\mathbf{B}^T\mathbf{G}_{b(n)}^T\mathbf{G}_{b(n)}\mathbf{R}_{w(n)}^{-1}\mathbf{A}).
\end{aligned} \tag{29}$$

The first term in this equation is constant. Therefore, we only need to maximize the $\mathrm{tr}(\mathbf{B}^T\mathbf{G}_{b(n)}^T\mathbf{G}_{b(n)}\mathbf{R}_{w(n)}^{-1}\mathbf{A})$ subject to the constraint $\mathbf{A}^T\mathbf{A} = \mathbf{I}$. The solution is obtained by computing the SVD

$$\mathbf{R}_{w(n)}^{-T}(\mathbf{G}_{b(n)}^T\mathbf{G}_{b(n)})\mathbf{B} = \mathbf{U}\mathbf{D}\mathbf{V}^T. \tag{30}$$

Given a fixed $\mathbf{B}$, the solution of (28) is $\hat{\mathbf{A}} = \mathbf{U}\mathbf{V}^T$ according to [30, Th. 4].

Given a fixed $\mathbf{A}$, let $\mathbf{A}_\perp$ be an orthogonal matrix such that $[\mathbf{A}; \mathbf{A}_\perp]$ is $I_n \times I_n$ orthogonal, where $[\mathbf{A}; \mathbf{A}_\perp]$ means to concatenate matrices $\mathbf{A}$ and $\mathbf{A}_\perp$ along rows. This is feasible since $\mathbf{A}$ has orthonormal columns. Thus the first term in (28) can be rewritten as following:

$$\begin{aligned}
&\sum_{i=1}^{\widetilde{I}_n} \|\mathbf{R}_{w(n)}^{-T}\mathbf{g}_i - \mathbf{A}\mathbf{B}^T\mathbf{g}_i\|^2 \\
&= \|\mathbf{G}_{b(n)}\mathbf{R}_{w(n)}^{-1} - \mathbf{G}_{b(n)}\mathbf{B}\mathbf{A}^T\|^2 \\
&= \|\mathbf{G}_{b(n)}\mathbf{R}_{w(n)}^{-1}[\mathbf{A}; \mathbf{A}_\perp] - \mathbf{G}_{b(n)}\mathbf{B}\mathbf{A}^T[\mathbf{A}; \mathbf{A}_\perp]\|^2 \\
&= \|\mathbf{G}_{b(n)}\mathbf{R}_{w(n)}^{-1}\mathbf{A} - \mathbf{G}_{b(n)}\mathbf{B}\|^2 + \|\mathbf{G}_{b(n)}\mathbf{R}_{w(n)}^{-1}\mathbf{A}_\perp\|^2 \\
&= \sum_{j=1}^{L_n} \|\mathbf{G}_{b(n)}\mathbf{R}_{w(n)}^{-1}\alpha_j - \mathbf{G}_{b(n)}\beta_j\|^2 + \|\mathbf{G}_{b(n)}\mathbf{R}_{w(n)}^{-1}\mathbf{A}_\perp\|^2.
\end{aligned} \tag{31}$$

Given a fixed $\mathbf{A}$, therefore, the solution of (28) is $\mathbf{B} = [\beta_1, \ldots, \beta_{L_n}]$, where β_j can be obtained by solving the following ridge regression problems:

$$\min_{\beta_j} \|\mathbf{G}_{b(n)}\mathbf{R}_{w(n)}^{-1}\alpha_j - \mathbf{G}_{b(n)}\beta_j\|^2 + \lambda\beta_j^T\mathbf{S}_w^{(n)}\beta_j. \tag{32}$$

Here, L_n ridge regression problems are independent to each other. In summary, we transform the generalized eigenvalue problem (17) to L_n ridge regression problems (32). However, the ridge regression does not provide a sparse solution. In order to get the sparse solutions, one can use lasso regression [36] on β_j by using ℓ_1 norm. Fig. 1 shows that the sparse solution can be found by solving a ℓ_1 norm problem but not by solving a traditional ℓ_2 norm problem.

We denote $\widetilde{\mathbf{y}}_j = (\mathbf{G}_{b(n)}\mathbf{R}_{w(n)}^{-1}\alpha_j, 0_{1\times I_n})^T$ and $\widetilde{\mathbf{W}} = (\mathbf{G}_{b(n)}^T, \sqrt{\lambda}\mathbf{R}_{w(n)}^T)^T$, the ridge regression problems (32) are equal to the following lasso regression problems:

$$\min_{\beta_j} \|\widetilde{\mathbf{y}}_j - \widetilde{\mathbf{W}}\beta_j\|^2 + \lambda_1\|\beta_j\|_1 \tag{33}$$

where λ_1 is the ℓ_1 norm tuning parameter. When λ_1 is large enough, some elements in β_j will be shrunk to zero. However, the lasso has several shortages as pointed out in [32]. For instance, the number of extracted features by the lasso is limited by the number of samples. To address the shortage, the elastic net [32] generalizes the lasso by combining both the ℓ_1 norm and ℓ_2 norm as the penalty. The lasso regression problems (33) can be written as the following elastic net

Algorithm 1 STDCS

INPUT: a set of M labeled tensor samples $\mathcal{A}_i^c$, $i = 1, 2, \ldots, M_c$, $c = 1, 2, \ldots, C$, the number of reduced dimensions L_n, $n = 1, 2, 3$ and sparse tuning parameters $\lambda, \lambda_1, \lambda_2$.

OUTPUT: a set of projected tensors $\mathcal{D}_i^c$, two sparse discriminant projection matrices $\mathbf{U}_1 \in \mathbb{R}^{I_1\times L_1}$, $\mathbf{U}_2 \in \mathbb{R}^{I_2\times L_2}$ and a sparse color space transformation matrix $\mathbf{U}_3 \in \mathbb{R}^{I_3\times L_3}$.

Algorithm:

Initialize $\mathbf{U}_n$ with a set of identity matrices;
Calculate the mean image of the cth individual $\overline{\mathcal{A}}^c$ and the mean image of all individuals $\overline{\mathcal{A}}$ by (7) and (8);
Calculate $\mathcal{H}_w$ and $\mathcal{H}_b$ by using (19);
repeat
  for $n = 1$ to 3 **do**
    Calculate $\mathcal{G}_w$ and $\mathcal{G}_b$ by (21) and (22);
    Calculate the mode-n unfolding $\mathbf{G}_{b(n)}$ and $\mathbf{G}_{w(n)}$;
    Calculate the upper triangular matrix $\mathbf{R}_{w(n)} \in \mathbb{R}^{I_n\times I_n}$ from the Cholesky decomposition of $\mathbf{G}_{w(n)}^T\mathbf{G}_{w(n)}$ such that $\mathbf{G}_{w(n)}^T\mathbf{G}_{w(n)} = \mathbf{R}_{w(n)}^T\mathbf{R}_{w(n)}$;
    Initialize $\mathbf{A}$ as an identity matrix;
    Calculate $\widetilde{\mathbf{W}} = (\mathbf{G}_{b(n)}^T, \sqrt{\lambda}\mathbf{R}_{w(n)}^T)^T$;
    repeat
      for $j = 1$ to L_n **do**
        Calculate $\widetilde{\mathbf{y}}_j = (\mathbf{G}_{b(n)}\mathbf{R}_{w(n)}^{-1}\alpha_j, 0_{1\times I_n})^T$;
        Solve $\min_{\beta_j} \|\widetilde{\mathbf{y}}_j - \widetilde{\mathbf{W}}\beta_j\|^2 + \lambda_{1,j}\|\beta_j\|_1 + \lambda_2\|\beta_j\|^2$ by using the elastic net;
      end for
      Calculate $\mathbf{B} = [\beta_1, \ldots, \beta_{L_n}]$;
      Calculate $\mathbf{R}_{w(n)}^{-T}(\mathbf{G}_{b(n)}^T\mathbf{G}_{b(n)})\mathbf{B} = \mathbf{U}\mathbf{D}\mathbf{V}^T$ by using SVD;
      Calculate $\mathbf{A} = \mathbf{U}\mathbf{V}^T$;
    until $norm(\mathbf{B}_{k'+1} - \mathbf{B}_{k'}) < \epsilon_1$
  end for
  Calculate $\mathbf{U}_n = \mathbf{B}$;
  Calculate J_{k+1} by (11);
until $|J_{k+1} - J_k| < \epsilon$
Compute a set of projected tensors $\mathcal{D}_i^c$ by (6).

Fig. 2. Sample images of one individual from the AR database.

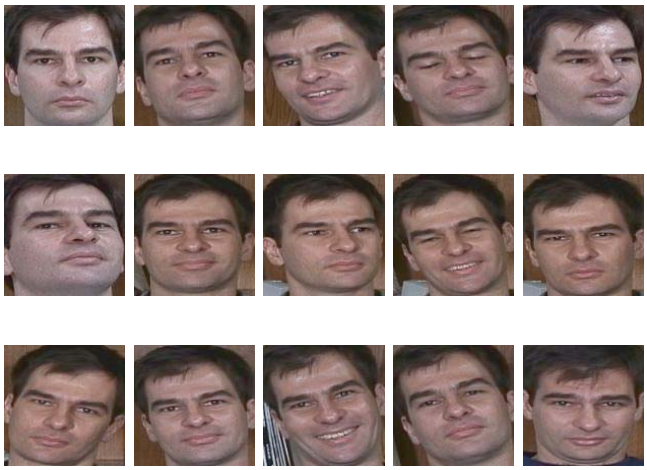

Fig. 3. Sample images of one individual from the Georgia Tech database (unaligned head images).

problems:

$$\min_{\beta_j} \|\widetilde{\mathbf{y}}_j - \widetilde{\mathbf{W}}\beta_j\|^2 + \lambda_{1,j}\|\beta_j\|_1 + \lambda_2\|\beta_j\|^2 \qquad (34)$$

where λ_2 is the ℓ_2 norm tuning parameter. When $\lambda_2 = 0$, elastic net is degraded to lasso regression.

Now, given all other sparse projection matrices $\mathbf{U}_1, \ldots, \mathbf{U}_{n-1}, \mathbf{U}_{n+1}, \ldots, \mathbf{U}_N$, the sparse solution $\mathbf{U}_n$ can be obtained by solving the L_n elastic net problems (34). Since the $\mathbf{G}_{b(n)}$ and $\mathbf{R}_{w(n)}$ depend on $\mathbf{U}_1, \ldots, \mathbf{U}_{n-1}, \mathbf{U}_{n+1}, \ldots, \mathbf{U}_N$, it can be seen that the optimization of $\mathbf{U}_n$ depends on the projections in other modes. An iterative procedure can be constructed to maximize (18). The pseudocode of the proposed method is summarized in Algorithm 1.

V. Experiments and Results

A. Database

We conducted the experiments on three well-known color face databases: AR [37], Georgia Tech face databases,[1] and LFW face databases.[2]

The AR database contains over 4000 color face images of 126 people (70 male and 56 female). A subset of 100 people (50 male and 50 female) were selected in our experiment. The selected images were frontal view faces with different facial expressions, illumination conditions, and occlusions (sun glasses and scarf). All images were taken under strictly controlled conditions. No restrictions on wear (clothes, glasses, etc.) make-up, hair style, etc. were imposed to participants. The same pictures were taken for each individual in two separate sessions, which were apart for two weeks. Twenty six images of each individual were selected in our experiment. All images were cropped into 32×32 pixels. The sample images of one individual from the AR database are shown in Fig. 2, where Fig. 2(a)–(m) is from the first session used as the training set, and Fig. 2(n)–(z) is from the second session used for testing purpose.

Georgia Tech face database contains images of 50 individuals, which were taken in two or three sessions at different times. For each individual in this database, 15 color JPEG images were captured with clutter backgrounds. The resolution of these images was 640×480 pixels and the size of face within these images was around 150×150. Faces illustrated in these images may be frontal and/or tilted with different expressions, illuminations, and scales. Each image was manually cropped and resized to 32×32 pixels. The sample images of one individual from the Georgia Tech database are showed in Fig. 3.

LFW database is designed for studying the problem of unconstrained face recognition. It contains more than 13 000 images of faces collected from the web. Each face has been labeled with the name of the person pictured. 1680 of the people pictured have two or more distinct photos in the data set. The only constraint on these faces is that they were detected by the Viola-Jones face detector. In our experiments, we choose 1251 images from 86 people pictured have 11–20 images. Each image was manually cropped and resized to 32×32 pixels. The sample images of one individual from the LFW database are showed in Fig. 4.

B. Experiment Setting

For the purpose of evaluating the performance of STDCS, we used *face verification rate* (FVR) as the criteria. The FERET verification testing protocol [38] recommends using the receiver operating characteristic (ROC) curves to depict the relations between the FVR and the false accept rate (FAR). In order to get better performance, in our experiments, the score matrices were generated by the Manhattan distance and Euclidean distance, respectively. The ROC curves were plotted by using the Statistical Learning Toolbox[3] according to the

[1] Available at http://www.anefian.com/research/face_reco.htm.

[2] Available at http://vis-www.cs.umass.edu/lfw/.

[3] The **slverifyroc** function in the Statistical Learning Toolbox can only plot the ROC curve illustrating the relations of the false reject rate versus the FAR. We modified it to depict the relations between the FVR and the FAR.

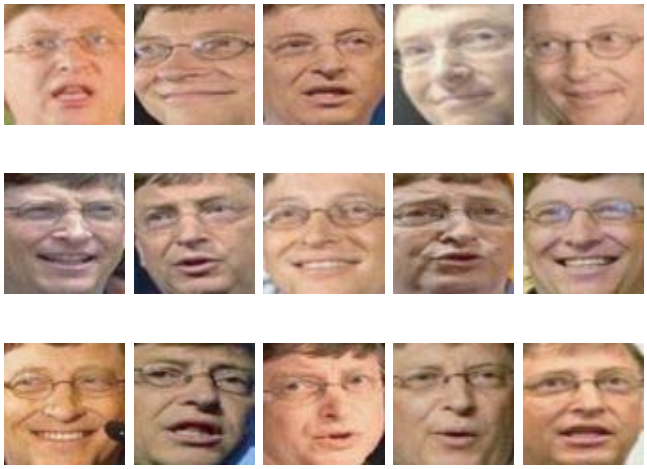

Fig. 4. Sample images of one individual from the LFW database.

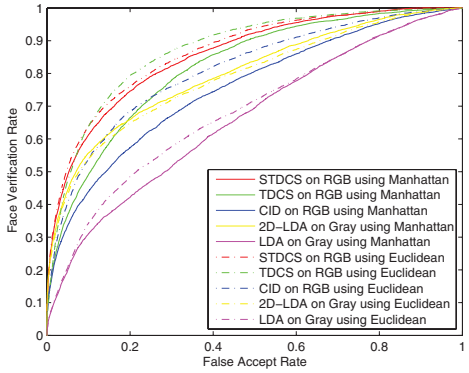

Fig. 5. ROC curves of STDCS, TDCS, CID, LDA, and LDA on the un-occluded facial images of AR database.

Fig. 6. Noise face images on the AR database.

obtained score matrix. For tensor operations, we used the tensor toolbox developed by Bader and Kolda in MATLAB [39]. All experiments on the Microsoft Windows XP 64-bits version machine with 2.66 GHz Intel CPU and 16 GB memory.

In our experiments, we will discuss the robustness of algorithms from the following two aspects.

1) The performance of algorithms is insensitive to the measures (Manhattan distance and Euclidean distance).
2) The performance of algorithms is insensitive to the aligned faces, occluded faces, and noised faces.

C. Experiments and Results on the AR Database

In this experiment, we trained STDCS, TDCS, and CID by using seven un-occluded color face images of each individual from the first session in AR database and tested them using the corresponding images in the second session. The convergence threshold ϵ was set as 0.1 and $\mathbf{x}_1$, was initialized as $[(1/3), (1/3), (1/3)]^T$. In STDCS, we set $\lambda = 1000$ and $\lambda_2 = 10^{-6}$. For the parameter λ_1, we used another strategy to tune the sparseness. The number of nonzero elements in each column of three sparse projection matrices was 10, 10, and 2. Meanwhile, we carried out LDA and 2-D-LDA on corresponding gray images. Because there were 100 individuals in the AR database, only 99 discriminant projection basis vectors were extracted in LDA and CID. For 2-D-LDA, TDCS, and STDCS, the two numbers of the reduced spatial dimensions both are 10. The score matrices were generated by Manhattan distance and Euclidean distance, respectively. The ROC curves of the five methods are shown in Fig. 5. The results indicate that the performance of TDCS with Euclidean distance is slightly better than that of STDCS with Manhattan distance. However, the space between two curves of STDCS is narrower than the space between two curves of TDCS. This shows that STDCS is more robust to the measures than TDCS. The curves in Fig. 5 also show that the 20 discriminant projection basis vectors in STDCS, and TDCS contain more discriminant information than 99 ones in CID. It is derived from the fact that some discriminant information is thrown away in the PCA step of CID model.

In order to investigate the robustness to noise, we used all images including the occluded facial images in the first session to train the models. All images in the second session were used for testing. In this case, we got three color space transformation matrices

$$\mathbf{X} = \begin{bmatrix} 0.4126 & -0.2107 & -0.5558 \\ -0.0261 & -0.4683 & 1.0536 \\ 1.0000 & 0.9739 & -0.5524 \end{bmatrix} \tag{35}$$

$$\mathbf{U}_3 = \begin{bmatrix} 0.1267 & -0.2084 & 0.3358 \\ -0.2128 & -0.4168 & -0.7897 \\ 0.9689 & 0.8848 & 0.5134 \end{bmatrix} \tag{36}$$

and

$$\mathbf{U}_3^{\text{sparse}} = \begin{bmatrix} 0.8270 & 0 & 0.2287 \\ 0.5622 & -0.9975 & 0.9735 \\ 0 & -0.0705 & 0 \end{bmatrix}. \tag{37}$$

There are two nonzero elements in each column of $\mathbf{U}_3^{\text{sparse}}$. Using these three matrices, we got three color components $\mathbf{D}^1$, $\mathbf{D}^2$, $\mathbf{D}^3$ of CID, three color components $\mathbf{T}^1$, $\mathbf{T}^2$, $\mathbf{T}^3$ of TDCS and three color components $\mathbf{S}^1$, $\mathbf{S}^2$, $\mathbf{S}^3$ of STDCS. These components are illustrated in Fig. 8. Compared to CID color space and TDCS color space, STDCS color space is more intuitionistic, i.e., the color component images of STDCS look more like real faces. Although $\mathbf{S}^1$ and $\mathbf{S}^3$ are similar to RGB space, the influence of light on R component in RGB is decreased in STDCS by the linear combination of R and G components. The ROC curves are illustrated in Fig. 9, where STDCS with Manhattan distance obtains the best performance. Comparing with Fig. 5, STDCS obtains the best performance for the occluded facial images. This also verify the STDCS robustness to the occluded facial images.

In order to further investigate the robustness to noise, some images were randomly selected and occluded with a rectangular noise consisting of random black and white dots whose size was at least 128 pixels, located at a random position. The manner of forming rectangle noise is similar to

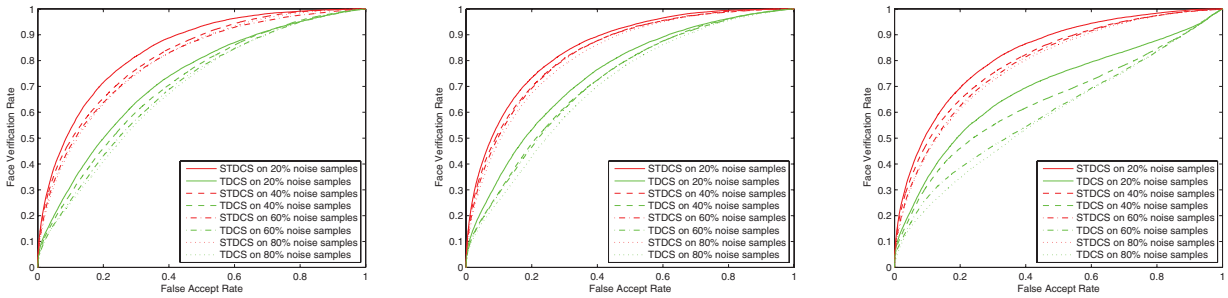

(a) (b) (c)

Fig. 7. ROC curves of STDCS and TDCS the noised facial images of AR database. (a) Noise on both training set and testing set. (b) Noise on training set. (c) Noise on testing set.

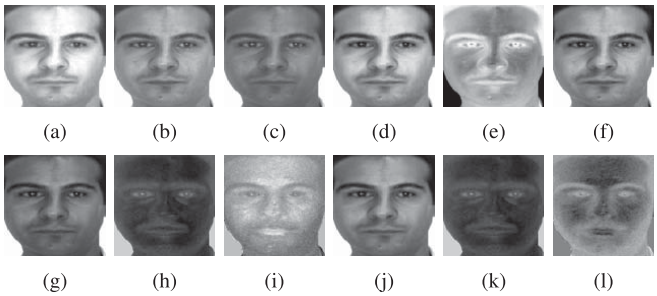

(a) (b) (c) (d) (e) (f)

(g) (h) (i) (j) (k) (l)

Fig. 8. Illustration of R, G, and B color components and the various components generated by CID, TDCS, and STDCS on the AR face database. (a) R. (b) G. (c) B. (d) S1. (e) S2. (f) S3. (g) T1. (h) T2. (i) T3. (j) D1. (k) D2. (l) D3.

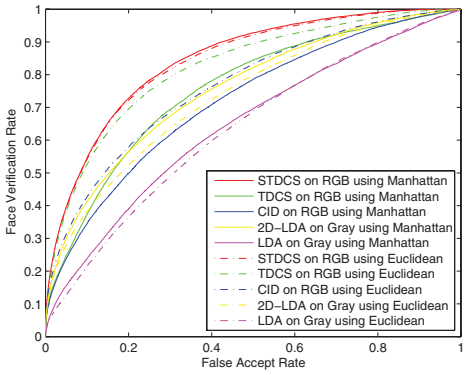

Fig. 9. ROC curves of STDCS, TDCS, CID, 2-D-LDA, and LDA on AR face database.

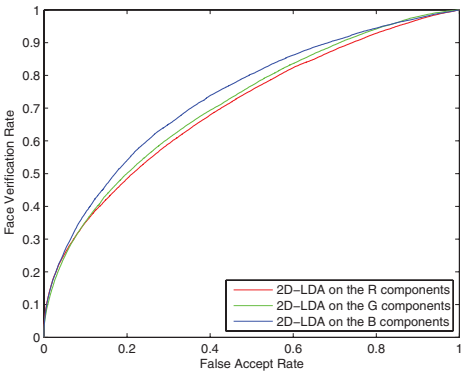

Fig. 10. ROC curves of 2-D-LDA on R, G, and B components of AR face database.

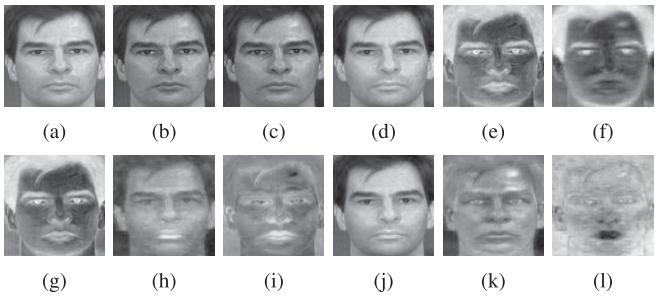

(a) (b) (c) (d) (e) (f)

(g) (h) (i) (j) (k) (l)

Fig. 11. Illustration of R, G, and B color components and the various components generated by CID, TDCS, and STDCS on the Georgia Tech face database. (a) R. (b) G. (c) B. (d) S1. (e) S2. (f) S3. (g) T1. (h) T2. (i) T3. (j) D1. (k) D2. (l) D3.

that in [40]. Fig. 6 shows typical examples of noised images. Fig. 7(a) shows the ROC curves of STDCS and TDCS by adding noise to 20, 40, 60, and 80% samples of both the training set and the testing set. Fig. 7(a) and (c) shows the ROC curves of the two algorithms by adding noise on the training set and the testing set, respectively. From the figures, the performances of STDCS with 80% noised samples are better than those of TDCS with 20% noised samples in the three cases. It is interesting that the shapes of ROC curves are changed in the case of adding noise on the testing set.

For the intuition, we enhanced the sparse constraint and got a sparse color sparse color transformation matrix as followings:

$$\mathbf{U}_3^{\text{sparse}'} = \begin{bmatrix} 1 & 0 & 0 \\ 0 & 1 & 0 \\ 0 & 0 & -1 \end{bmatrix}. \tag{38}$$

Intuitively, the effect of B component differs from the other two. In order to verify this difference, 2-D-LDA is implemented on R, G and B component images, respectively. In Fig. 10, three ROC curves are illustrated from which we can see that the curves of R and G components are similar, while the curve of B component is quite different.

(a) (b) (c)

Fig. 12. Illustration of three color components $\mathbf{S}^1$, $\mathbf{S}^2$, $\mathbf{S}^3$ in STDCS on the Georgia Tech face database. (a) S1. (b) S2. (c) S3.

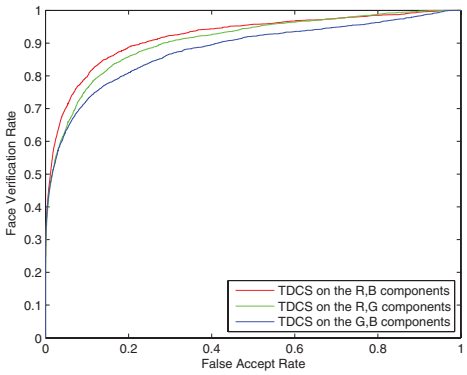

Fig. 13. ROC curves of TDCS on (R, B), (R, G), and (G, B) combinations.

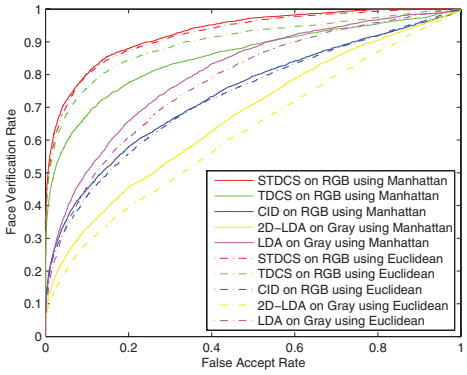

Fig. 14. ROC curves of TDCS, CID, 2-D-LDA, and LDA on the Georgia Tech face database.

D. Experiments and Results on the Georgia Tech Face Database

Georgia Tech face database is more complex than AR database, because it contains various pose faces with different expressions on cluttered background. In this experiment, we used the first eight images of each individual as the training set and the remaining images as the testing set. The CID, TDCS, and STDCS models were trained and we got three color space transformation matrices

$$\mathbf{X} = \begin{bmatrix} -1.0000 & 0.4894 & 0.4076 \\ 0.8473 & 0.3595 & -1.0134 \\ -0.2767 & -1.0401 & 0.5332 \end{bmatrix} \tag{39}$$

$$\mathbf{U}_3 = \begin{bmatrix} 0.1067 & -0.3004 & 0.6192 \\ 0.7589 & 0.7798 & -0.7852 \\ -0.6424 & -0.5492 & 0.0080 \end{bmatrix} \tag{40}$$

Fig. 15. Sample images for one individual of the Georgia Tech database (aligned facial images).

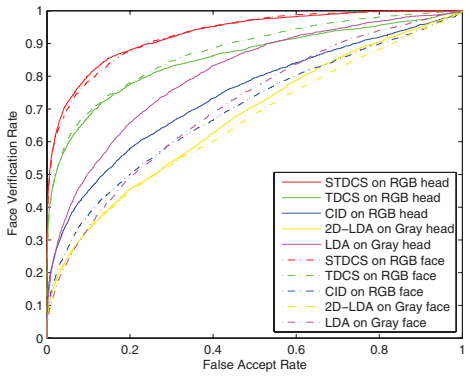

Fig. 16. ROC curves of TDCS, CID, 2-D-LDA, and LDA on the Georgia Tech face database.

Fig. 17. Noise face images on the Georgia Tech face database.

and

$$\mathbf{U}_3^{\text{sparse}} = \begin{bmatrix} 0.9051 & 0 & -0.7533 \\ -0.4252 & -0.7941 & 0 \\ 0 & 0.6077 & 0.6576 \end{bmatrix}. \tag{41}$$

These three matrices are not the same as (35)–(37) due to the different training sets. Using these three matrices, we got three color components $\mathbf{D}^1$, $\mathbf{D}^2$, $\mathbf{D}^3$ of CID; three color components $\mathbf{T}^1$, $\mathbf{T}^2$, $\mathbf{T}^3$ of TDCS and three color components $\mathbf{S}^1$, $\mathbf{S}^2$, $\mathbf{S}^3$ of STDCS. These components are illustrated in Fig. 11. In order to investigate the semantic interpretation of each color component, we set the number of nonzero elements in each column of the sparse color space transformation matrix as one. The matrix is obtained as

$$\mathbf{U}_3^{\text{sparse}'} = \begin{bmatrix} 1 & 0 & 0 \\ 0 & 0 & 0 \\ 0 & 1 & -1 \end{bmatrix}. \tag{42}$$

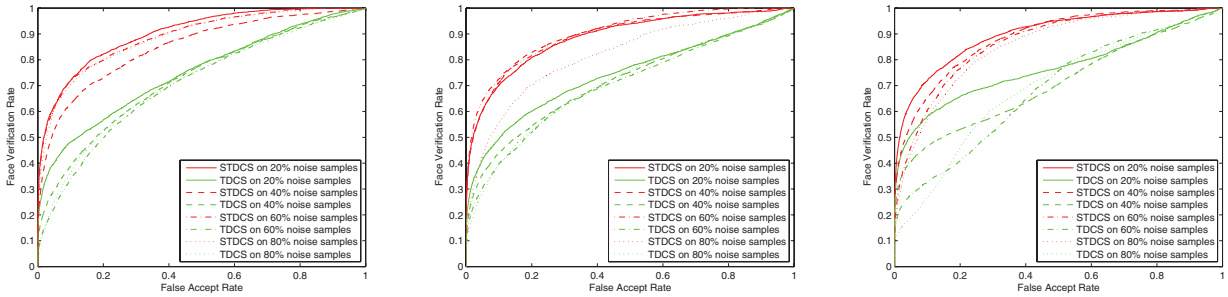

(a) (b) (c)

Fig. 18. ROC curves of STDCS and TDCS the noised facial images of the Georgia Tech face database. (a) Noise on both training set and testing. (b) Noise on training set. (c) Noise on testing set.

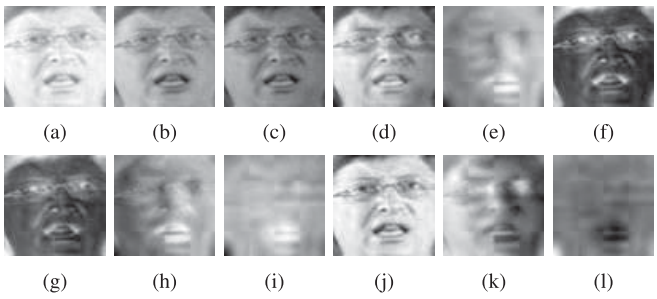

(a) (b) (c) (d) (e) (f)

(g) (h) (i) (j) (k) (l)

Fig. 19. Illustration of R, G, and B color components and the various components generated by CID, TDCS, and STDCS on the LFW face database. (a) R. (b) G. (c) B. (d) S1. (e) S2. (f) S3. (g) T1. (h) T2. (i) T3. (j) D1. (k) D2. (l) D3.

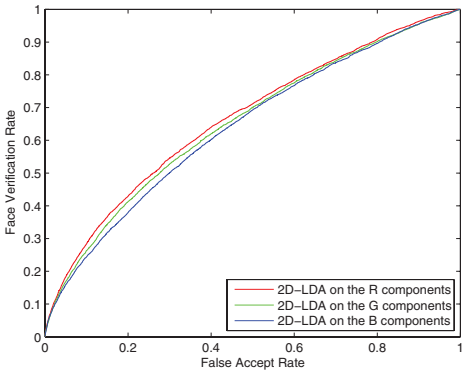

Fig. 20. ROC curves of 2-D-LDA on R, G, and B components of LFW face database.

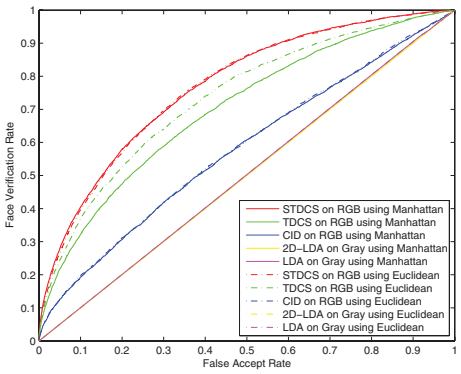

Fig. 21. ROC curves of STDCS, TDCS, CID, 2-D-LDA, and LDA on the LFW face database.

Fig. 12 illustrates three color components $\mathbf{S}^1$, $\mathbf{S}^2$, $\mathbf{S}^3$ in STDCS. The three components $\mathbf{S}^1$, $\mathbf{S}^2$, $\mathbf{S}^3$ come from R, B, and negative B components in RGB color space. From above analysis, the combination of R, B components from RGB space is most effective for facial recognition on Georgia Tech face database. The same conclusion can also be drawn from the matrix $\mathbf{U}_3^{\text{sparse}'}$. In order to verify this, TDCS was conducted on three different combinations of (R, B), (R, G), and (G, B), respectively. The score matrix was generated by using Euclidean distance. The ROC curves are illustrated in Fig. 13, where the ROC curve of the combination of (R, B) shows better performance than other two combinations.

To 50 individuals in the Georgia Tech database, 49 discriminant projection basis vectors were extracted using LDA and CID. For 2-D-LDA, TDCS, and STDCS, the two numbers of the reduced spatial dimensions were both ten. In this experiment, the score matrices were generated by using Manhattan distance and Euclidean distance, respectively. In Fig. 14, Manhattan distance and Euclidean distance are denoted by solid lines and dash-dot lines. The results indicate that STDCS has the best performance compared to other four algorithms. For TDCS, the performance of using Euclidean distance is better than that of using Manhattan distance. While for STDCS, the performance of using Euclidean distance is worse than that of using Manhattan distance. Even though the score matrix was generated by the Euclidean distance, the performance of STDCS is better than that of TDCS. From this figure, we can also see that the space between two curves of STDCS is narrower than that between two curves of TDCS. This shows that the STDCS is more insensitive to similarity measurement of images than TDCS.

In order to investigate robustness of models, all images in the Georgia Tech database were manually aligned (two eyes were used for alignment), cropped, and then re-sized to 32×32 pixels. To the cropped images as shown in Fig. 15, we retained as much of the facial region as possible, by eliminating most of the non-facial regions. The experiments with the same setting described above were conducted on them. The score matrix is generated by using Manhattan distance.

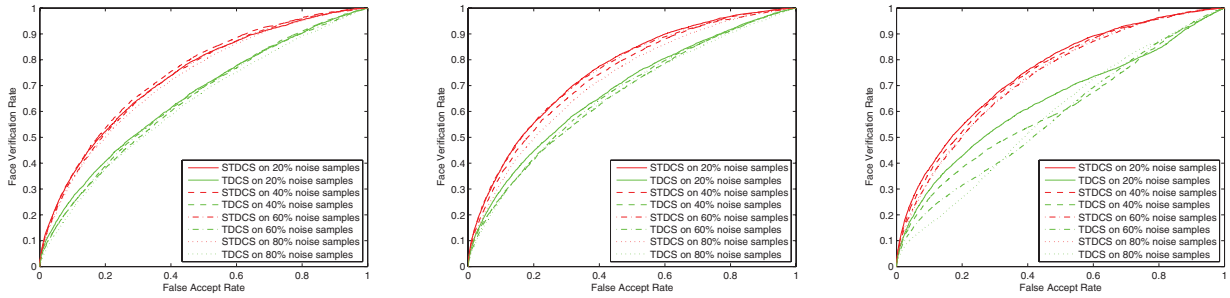

(a) (b) (c)

Fig. 22. ROC curves of STDCS and TDCS the noised facial images of LFW database. (a) Noise on both training set and testing set. (b) Noise on training set. (c) Noise on testing set.

The results of aligned facial images and unaligned head images are plotted and compared in Fig. 16. The solid lines denote the ROC curves on the unaligned head images, and the dash-dot lines denote the ROC curves on the aligned facial images. Generally, the performance on the aligned facial images should be better than the performance on the unaligned head image. However, image vector-based methods, such as CID and LDA, achieve opposite results where unaligned image provides better performance than aligned image. This is due to the fact that vectorization causes loss of the spatial structure information of images. Comparing three color space models, we can also see that the performances of STDCS and TDCS are better than that of CID. Furthermore, the margin between two curves of STDCS (or TDCS) is narrower than the margin between two curves of CID. Among them, the two ROC curves of STDCS are almost overlapped. This indicates that STDCS is more robust than TDCS and CID for the color images. This also shows that ℓ_1 norm is more robust than ℓ_2 norm [40].

In order to further investigate the robustness to noise, the noises are added on the Georgia Tech face database by using the same manner. Fig. 17 shows typical examples of noised images. Fig. 18 shows the ROC curves of the two algorithms in the three cases. The similar conclusions are drawn from the figure. It is interesting that the performance of STDCS with 60% noised training samples is the best.

E. Experiments and Results on the LFW Face Database

LFW database is designed for studying the problem of unconstrained face recognition. From Fig. 4, we can see that the skin color of the same person is different due to various cameras. In this experiment, we randomly selected $\lfloor p/2 \rfloor$ images of each person (the person has p images) as the training set and the remaining images as the testing set. The CID, TDCS, and STDCS models were trained and we got three color space transformation matrices

$$\mathbf{X} = \begin{bmatrix} 1.0000 & -1.0089 & -0.3600 \\ 0.3166 & 0.2805 & 0.9981 \\ -0.2236 & 0.9078 & -0.6621 \end{bmatrix} \tag{43}$$

$$\mathbf{U}_3 = \begin{bmatrix} -0.9103 & 0.6923 & 0.1885 \\ 0.4085 & -0.7043 & -0.7688 \\ -0.0673 & -0.1571 & 0.6111 \end{bmatrix} \tag{44}$$

and

$$\mathbf{U}_3^{\text{sparse}} = \begin{bmatrix} 0 & 0.6733 & -0.9736 \\ -0.4744 & -0.7394 & 0 \\ 0.8803 & 0 & 0.2281 \end{bmatrix}. \tag{45}$$

Using these three matrices, we got three color components $\mathbf{D}^1$, $\mathbf{D}^2$, $\mathbf{D}^3$ of CID; three color components $\mathbf{T}^1$, $\mathbf{T}^2$, $\mathbf{T}^3$ of TDCS and three color components $\mathbf{S}^1$, $\mathbf{S}^2$, $\mathbf{S}^3$ of STDCS. These components are illustrated in Fig. 19. Intuitively, the components of STDCS are more clear than those of TDCS and CID. In order to further investigate the semantic interpretation of each color component, we set the number of nonzero elements in each column of the sparse color space transformation matrix as one. The matrix is obtained as

$$\mathbf{U}_3^{\text{sparse}'} = \begin{bmatrix} 1 & 0 & 0 \\ 0 & 1 & 0 \\ 0 & 0 & 1 \end{bmatrix}. \tag{46}$$

From the above equation, we can see that each component plays the same role. By the same way, 2-D-LDA is implemented on R, G, and B components to verify the Intuition. In Fig. 20, three ROC curves are illustrated from which we can see that the curves of R, G, and B components are similar.

In the same way, STDCS, TDCS, CID, 2-D-LDA, and LDA are conducted on the LFW face database. Due to 86 individuals in the LFW database, LDA and CID only extract 85 discriminant projection basis vectors. Other parameters are the same with previous section. The results indicate that STDCS has the best performance compared to other four algorithms from Fig. 21. Comparing with TDCS, two curves of STDCS are overlapped. This shows that the STDCS is more insensitive to similarity measurement of images than TDCS. We can also see that the curves of the algorithms for gray images are almost consistent and their performance is the worst. It reveals that gray information is not enough for the discrimination of color images in this more complex case.

Similar noised experiments are conducted on LFW database. The results are illustrated in Fig. 22. Similar conclusions are drawn from the figure.

VI. Conclusion

In this paper, we presented a new color space model that was named as the STDCS. By learning from training samples, the

proposed model optimizes one sparse color space transformation matrix and two sparse discriminant projection matrices simultaneously. The experiments on the AR, Georgia Tech, and LFW color face databases were systematically performed and analyzed. The experimental results reveal a number of interesting remarks.

1) STDCS model can give an intuitionistic or semantic interpretation.
2) STDCS is more robust not only for similarity measurement of images but also for image alignments.

Our future work will be on the theoretical analysis of convergence of the algorithm.

REFERENCES

[1] M. Turk and A. Pentland, "Eigenfaces for recognition," *J. Cognit. Neurosci.*, vol. 3, no. 1, pp. 71–86, Jan. 1991.

[2] P. N. Belhumeur, J. P. Hespanha, and D. J. Kriegman, "Eigenfaces versus Fisherfaces: Recognition using class specific linear projection," *IEEE Trans. Pattern Anal. Mach. Intell.*, vol. 19, no. 7, pp. 711–720, Jul. 1997.

[3] J. Yang, D. Zhang, A. F. Frangi, and J. Y. Yang, "2-D PCA: A new approach to appearance-based face representation and recognition," *IEEE Trans. Pattern Anal. Mach. Intell.*, vol. 26, no. 1, pp. 131–137, Jan. 2004.

[4] M. Li and B. Z. Yuan, "2-D-LDA: A statistical linear discriminant analysis for image matrix," *Pattern Recognit. Lett.*, vol. 26, no. 5, pp. 527–532, 2005.

[5] M. A. O. Vasilescu and D. Terzopoulos, "Multilinear analysis of image ensembles: Tensorfaces," in *Proc. 7th Eur. Conf. Comput. Vis. I*, 2002, pp. 447–460.

[6] S. Park and M. Savvides, "Individual kernel tensor-subspaces for robust face recognition: A computationally efficient tensor framework without requiring mode factorization," *IEEE Trans. Syst., Man, Cybern., B, Cybern.*, vol. 37, no. 5, pp. 1156–1166, Oct. 2007.

[7] S.-J. Wang, C.-G. Zhou, Y.-H. Chen, X.-J. Peng, H.-L. Chen, G. Wang, and X. Liu, "A novel face recognition method based on sub-pattern and tensor," *Neurocomputing*, vol. 74, no. 17, pp. 3553–3564, 2011.

[8] L. De Lathauwer, B. De Moor, and J. Vandewalle, "On the best rank-1 and rank-(R_1, R_2, ..., R_N) approximation of higher-order tensors," *SIAM J. Matrix Anal. Appl.*, vol. 21, no. 4, pp. 1324–1342, 2000.

[9] L. De Lathauwer, B. De Moor, and J. Vandewalle, "A multilinear singular value decomposition," *SIAM J. Matrix Anal. Appl.*, vol. 21, no. 4, pp. 1253–1278, 2000.

[10] T. G. Kolda and B. W. Bader, "Tensor decompositions and applications," *SIAM Rev.*, vol. 51, no. 3, pp. 455–500, 2009.

[11] J. Ye, "Generalized low rank approximations of matrices," *Mach. Learn.*, vol. 61, no. 1, pp. 167–191, 2005.

[12] X. He, D. Cai, and P. Niyogi, "Tensor subspace analysis," in *Advances in Neural Information Processing Systems 18 (NIPS)*. Cambridge, MA: MIT Press, 2005.

[13] H. P. Lu, N. P. Konstantinos, and A. N. Venetsanopoulos, "MPCA: Multilinear principal component analysis of tensor objects," *IEEE Trans. Neural Netw.*, vol. 19, no. 1, pp. 18–39, Jan. 2008.

[14] S.-J. Wang, C.-G. Zhou, N. Zhang, X.-J. Peng, Y.-H. Chen, and X. Liu, "Face recognition using second-order discriminant tensor subspace analysis," *Neurocomputing*, vol. 74, nos. 12–13, pp. 2142–2156, Jun. 2011.

[15] X. F. He and P. Niyogi, "Locality preserving projections," in *Advances in Neural Information Processing Systems 16*, vol. 16. Cambridge, MA: MIT Press, 2004, pp. 153–160.

[16] N. Kumar, P. Belhumeur, and S. Nayar, "Facetracer: A search engine for large collections of images with faces," in *Proc. 10th Eur. Conf. Comput. Vis. IV*, 2008, pp. 340–353.

[17] J. Wright, A. Yang, A. Ganesh, S. Sastry, and Y. Ma, "Robust face recognition via sparse representation," *IEEE Trans. Pattern Anal. Mach. Intell.*, vol. 31, no. 2, pp. 210–227, Feb. 2009.

[18] W. Schwartz, H. Guo, and L. Davis, "A robust and scalable approach to face identification," in *Proc. Eur. Conf. Comput. Vis.*, 2010, pp. 476–489.

[19] Z. Fan, Y. Xu, and D. Zhang, "Local linear discriminant analysis framework using sample neighbors," *IEEE Trans. Neural Netw.*, vol. 22, no. 7, pp. 1119–1132, Jul. 2011.

[20] S. Zafeiriou, G. Tzimiropoulos, M. Petrou, and T. Stathaki, "Regularized kernel discriminant analysis with a robust kernel for face recognition and verification," *IEEE Trans. Neural Netw. Learn. Syst.*, vol. 23, no. 3, pp. 526–534, Mar. 2012.

[21] L. Torres, J. Reutter, and L. Lorente, "The importance of the color information in face recognition," in *Proc. Int. Conf. Image Process.*, vol. 3. 1999, pp. 627–631.

[22] C. Wang, B. Yin, X. Bai, and Y. Sun, "Color face recognition based on 2-DPCA," in *Proc. 19th Int. Conf. Pattern Recognit.*, 2008, pp. 1–4.

[23] J. Choi, Y. Ro, and K. Plataniotis, "Color face recognition for degraded face images," *IEEE Trans. Syst., Man, Cybern., B, Cybern.*, vol. 39, no. 5, pp. 1217–1230, Oct. 2009.

[24] M. Villegas, R. Paredes, A. Juan, and E. Vidal, "Face verification on color images using local features," in *Proc. IEEE Comput. Soc. Conf. Comput. Vis. Pattern Recognit. Workshops*, Jun. 2008, pp. 1–6.

[25] W. H. Buchsbaum, *Color TV Servicing*, 3rd ed. Englewood Cliffs, NJ: Prentice-Hall, 1975.

[26] K. Fukunaga, *Introduction to Statistical Pattern Recognition*. New York: Academic, 1990.

[27] C. Liu, "Learning the uncorrelated, independent, and discriminating color spaces for face recognition," *IEEE Trans. Inf. Forens. Secur.*, vol. 3, no. 2, pp. 213–222, Jun. 2008.

[28] J. Yang and C. Liu, "Color image discriminant models and algorithms for face recognition," *IEEE Trans. Neural Netw.*, vol. 19, no. 12, pp. 2088–2098, Dec. 2008.

[29] S.-J. Wang, J. Yang, N. Zhang, and C.-G. Zhou, "Tensor discriminant color space for face recognition," *IEEE Trans. Image Process.*, vol. 20, no. 9, pp. 2490–2501, Sep. 2011.

[30] H. Zou, T. Hastie, and R. Tibshirani, "Sparse principal component analysis," *J. Comput. Graph. Stat.*, vol. 15, no. 2, pp. 265–286, 2006.

[31] B. Efron, T. Hastie, I. Johnstone, and R. Tibshirani, "Least angle regression," *Ann. Stat.*, vol. 32, no. 2, pp. 407–499, 2004.

[32] H. Zou and T. Hastie, "Regression shrinkage and selection via the elastic net, with applications to microarrays," *J. Royal Stat. Soc. B*, vol. 67, pp. 301–320, 2005.

[33] B. Moghaddam, Y. Weiss, and S. Avidan, "Spectral bounds for sparse PCA: Exact and greedy algorithms," in *Advances in Neural Information Processing Systems*, vol. 18. Cambridge, MA: MIT Press, 2006, p. 915.

[34] B. Moghaddam, Y. Weiss, and S. Avidan, "Generalized spectral bounds for sparse LDA," in *Proc. 23rd Int. Conf. Mach. Learn.*, 2006, pp. 641–648.

[35] Z. Qiao, L. Zhou, and J. Z. Huang, "Sparse linear discriminant analysis with applications to high dimensional low sample size data," *IAENG Int. J. Appl. Math.*, vol. 39, no. 1, pp. 48–60, 2009.

[36] T. Hastie, R. Tibshirani, and J. Friedman, *The Elements of Statistical Learning: Data Mining, Inference, and Prediction*. New York: Springer-Verlag, 2001.

[37] A. Martinez and R. Benavente, "The AR face database," Centre de Visió per Computador, Univ. Purdue, West Lafayette, IN, Tech. Rep. 24, 1998.

[38] H. Moon and P. Phillips, "The FERET verification testing protocol for face recognition algorithms," in *Proc. 3rd IEEE Int. Autom. Face Gesture Recognit.*, 1998, pp. 48–53.

[39] B. Bader and T. G. Kolda. *Tensor Toolbox Version 2.3*. Sandia National Laboratories, Albuquerque, NM [Online]. Available: http://csmr.ca.sandia.gov/~tgkolda/TensorToolbox/

[40] N. Kwak, "Principal component analysis based on L1-norm maximization," *IEEE Trans. Pattern Anal. Mach. Intell.*, vol. 30, no. 9, pp. 1672–1680, Sep. 2008.

Su-Jing Wang received the Masters degree from the Software College, Jilin University, Changchun, China, in 2007. He is currently pursuing the Ph.D. degree with the College of Computer Science and Technology, Jilin University.

He has published more than 30 scientific papers. He was called a "Chinese Hawking" by the Xinhua News Agency. His research was published in the IEEE TRANSACTIONS ON IMAGE PROCESSING and *Neurocomputing*. His current research interests include pattern recognition, computer vision, and machine learning.

Mr. Wang is the One of Ten Selectees of the Doctoral Consortium at International Joint Conference on Biometrics in 2011. He reviews for several top journals, such as the IEEE TRANSACTIONS ON PATTERN ANALYSIS AND MACHINE INTELLIGENCE and the IEEE TRANSACTIONS ON NEURAL NETWORKS AND LEARNING SYSTEMS.

Jian Yang (M'08) received the B.S. degree in mathematics from Xuzhou Normal University, Xuzhou, China, in 1995, the M.S. degree in applied mathematics from Changsha Railway University, Hunan, China, in 1998, and the Ph.D. degree from the Nanjing University of Science and Technology (NUST), Nanjing, China, in 2002, focused on the pattern recognition and intelligence systems.

He was a Post-Doctoral Researcher with the University of Zaragoza, Saragossa, Spain, in 2003. He was a Post-Doctoral Fellow with the Biometrics Center, Hong Kong Polytechnic University, Hong Kong, from 2004 to 2006, and the Department of Computer Science, New Jersey Institute of Technology, Newark, from 2006 to 2007. He is currently a Professor with the School of Computer Science and Technology, NUST. He is the author of more than 50 scientific papers in pattern recognition and computer vision. His current research interests include pattern recognition, computer vision, and machine learning.

Dr. Yang received the RyC Program Research Fellowship sponsored by the Spanish Ministry of Science and Technology in 2003. He is currently an Associate Editor of *Pattern Recognition Letters* and the IEEE TRANSACTIONS ON NEURAL NETWORKS AND LEARNING SYSTEMS.

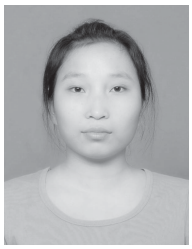

Ming-Fang Sun received the B.E. degree in computer science and technology from Jilin University, Changchun, China, in 2009. She is currently pursuing the Masters degree with the College of Computer Science and Technology, Jilin University.

Her current research interests include face recognition and human action recognition.

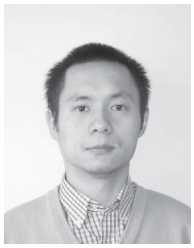

Xu-Jun Peng received the Ph.D. degree from the Department of Computer Science and Engineering, State University of New York, Buffalo.

He is currently a Research Scientist with Raytheon BBN Technologies, Cambridge, MA. His current research interests include machine learning, image processing, and document analysis.

Ming-Ming Sun received the B.S. degree in mathematics from Xinjiang University, Urumqi, China, in 2002, and the Ph.D. degree in pattern recognition and intelligence systems from the Department of Computer Science, Nanjing University of Science and Technology (NUST), Nanjing, China, in 2007.

He is currently a Lecturer with the School of Computer Science and Technology, NUST. His current research interests include pattern recognition, machine learning, and image processing.

Chun-Guang Zhou received the Ph.D. degree from the Institute of Computer Science, Jilin University, Changchun, China.

He is a Professor, a Ph.D. Supervisor, and the Dean of the Institute of Computer Science, Jilin University. He is a Jilin-Province-Management Expert, a highly qualified expert of the Jilin Province, and One-hundred Science-Technique Elite of Changchun. He has many pluralities of national and international academic organizations. He has published over 168 papers in journals and conferences. He has published one academic book. His current research interests include related theories, models and algorithms of artificial neural networks, fuzzy systems and evolutionary computation, applications of machine taste and smell, image manipulation, commercial intelligence, modern logistic, bioinformatics, and biometric identification based on computational intelligence.

Dr. Zhou received the Governmental Subsidy from the State Department.